

# Dual-comb Photothermal Spectroscopy

**Qiang Wang** (✉ [wangqiang@ciomp.ac.cn](mailto:wangqiang@ciomp.ac.cn))

Changchun Institute of Optics, Fine Mechanics and Physics, Chinese Academy of Sciences  
<https://orcid.org/0000-0001-9875-7500>

**Zhen Wang**

Changchun Institute of Optics, Fine Mechanics and Physics, Chinese Academy of Sciences

**Hui Zhang**

Changchun Institute of Optics, Fine Mechanics and Physics, Chinese Academy of Sciences

**Shoulin Jiang**

The Hong Kong Polytechnic University

**Yingying Wang**

Jinan University, Guangzhou

**Wei Jin**

The Hong Kong Polytechnic University

**Wei Ren**

The Chinese University of Hong Kong <https://orcid.org/0000-0001-6681-593X>

---

## Article

### Keywords:

**Posted Date:** December 3rd, 2021

**DOI:** <https://doi.org/10.21203/rs.3.rs-1106913/v1>

**License:**   This work is licensed under a Creative Commons Attribution 4.0 International License.

[Read Full License](#)

---

**Version of Record:** A version of this preprint was published at Nature Communications on April 21st, 2022. See the published version at <https://doi.org/10.1038/s41467-022-29865-6>.

## Dual-comb Photothermal Spectroscopy

Qiang Wang<sup>1,2,†,\*</sup>, Zhen Wang<sup>3,†,\*</sup>, Hui Zhang<sup>1,2</sup>, Shoulin Jiang<sup>4</sup>, Yingying Wang<sup>5</sup>, Wei Jin<sup>4</sup>, and Wei Ren<sup>3,\*</sup>

<sup>1</sup>State Key Laboratory of Applied Optics, Changchun Institute of Optics, Fine Mechanics and Physics, Chinese Academy of Sciences, Changchun 130033, China

<sup>2</sup>University of Chinese Academy of Sciences, Beijing 100049, China

<sup>3</sup>Department of Mechanical and Automation Engineering, and Shenzhen Research Institute, The Chinese University of Hong Kong, New Territories, Hong Kong SAR, China

<sup>4</sup>Department of Electrical Engineering, The Hong Kong Polytechnic University, Kowloon, Hong Kong SAR, China.

<sup>5</sup>Institute of Photonics Technology, Jinan University, Guangzhou 510632, China

<sup>†</sup>These authors contributed equally to this work

\*Email: wangqiang@ciomp.ac.cn; wangzhen@link.cuhk.edu.hk; renwei@mae.cuhk.edu.hk

Dual-comb spectroscopy (DCS) has revolutionized optical spectroscopy by providing broadband spectral measurements with unprecedented resolution and fast response. Photothermal spectroscopy (PTS) offers an ultrasensitive and background-free gas sensing method, which is normally performed using a single-wavelength pump laser. The merging of PTS with DCS may enable a new spectroscopic method by taking advantage of both technologies, which has never been studied yet. Here, we report dual-comb photothermal spectroscopy (DC-PTS) by passing dual combs and a probe laser through a gas-filled anti-resonant hollow-core fiber, where the generated multi-heterodyne modulation of the refractive index is sensitively detected by an in-line interferometer. As an example, we have measured photothermal spectra of acetylene over 1 THz, showing a good agreement with the spectral database. Our proposed DC-PTS provides new opportunities for broadband gas sensing with super-fine resolution and high sensitivity, as well as with a small sample volume and compact configuration.

Optical frequency combs (OFCs) have significantly promoted the development of many research fields in the past decades such as time and frequency metrology [1,2], attosecond science [3], optical communication [4] and precision spectroscopy [5,6]. This light source presents an optical spectrum composed of a set of evenly spaced and phase-coherent laser lines. The combination of broad spectral bandwidth and high spectral resolution makes OFCs particularly suitable for high-precision molecular spectroscopy and multi-species gas detection. Among different OFC-based spectroscopic methods [7–12], dual-comb spectroscopy (DCS) provides a versatile approach to Fourier transform interferometry without any moving parts, leading to many advantages such as high resolution, short acquisition time, high signal-to-noise ratio and free from size constraints.

DCS is mostly conducted with absorption spectroscopy that a broadband photodetector is used to measure the comb transmission through the gas medium. Hence, this technique requires a long mutual coherence time for averaging and a long light-gas interaction path to enhance the detection sensitivity. The mutual coherence time between two combs has approached 1860 s with the feed-forward locking technique [13]. Although DCS has been demonstrated with different kinds of comb sources, most studies used a short single-pass gas cell with high-concentration gas

samples just for demonstration purposes [14–18]. It is possible to increase the effective path length using a multipass gas cell or an optical cavity [12,19]. However, the multipass cell with large mirrors has a bulky size. The optical loss per reflection also limits the use of low-power OFCs [20]. In comparison, an optical cavity can increase the optical path by orders of magnitude with less optical loss. Cavity-enhanced dual-comb spectroscopy has been reported with ultra-high sensitivity [12,21,22], which requires complex optical setup and feedback control electronics to achieve the so-called two-point locking [11]. The spectral bandwidth may also be constrained by the dispersion issue of cavity mirrors. Hence, new strategies are demanding for DCS that can achieve broadband, high-resolution and ultrasensitive detection in a compact system. Photoacoustic spectroscopy (PAS), an indirect absorption detection method, has been recently explored by several research groups using OFCs [23–26]. Based on a Fourier transform spectrometer with a comb source, researchers measured broadband photoacoustic spectra of methane using a micro-cantilever [23–24]. Very recently, dual-comb PAS has been demonstrated for measuring acetylene [25] and polymer films [26]. These methods provide an alternative way of spectroscopic measurements of gases, liquids and even solids.

Interestingly, photothermal spectroscopy (PTS) is another important method widely used in spectroscopy and microscopy [27–30]. In PTS, the modulated light absorption generates periodic heating of a gas sample, resulting in the variation of gas density and refractive index (RI). As the photothermal effect is quite sensitive to the laser intensity, it is quite promising to perform ultrasensitive PTS in a hollow-core fiber (HCF) with a small mode field diameter (MFD) [27,29]. For instance, by using a hollow-core photonic bandgap fiber with a MFD of 11  $\mu\text{m}$ , an optical intensity of 40  $\text{kWcm}^{-2}$  can be obtained for an input power of 15.3 mW [27]. Additionally, photothermal spectroscopy is a background-free method for chemical analysis. A pump-probe configuration is often adopted for PTS, where the RI change induced by the pump laser is detected by an interferometer with a probe laser. Rather than performing photothermal detection with a single-wavelength pump laser, PTS combined with the dual-comb source has the potential to achieve a compact gas sensor with background-free, ultra-high sensitivity, and broadband detection, which has never been realized previously.

In this work, a new technique of dual-comb photothermal spectroscopy (DC-PTS) is reported. We use an electro-optic dual-comb source to generate the photothermal effect, which is sensitively detected by an in-line Fabry-Pérot interferometer (FPI). Such a highly versatile all-fiber sensing configuration is described in detail. Our experimental results reveal the current DC-PTS can provide tooth-resolved photothermal measurements of the  $(\nu_1+\nu_3)$  band of acetylene ( $\text{C}_2\text{H}_2$ ), spanning over 1 THz. With an average optical power of 15 mW for the dual-comb source, we achieve a minimum detection limit of 8.7 ppm  $\text{C}_2\text{H}_2$  over the coherent averaging time of 1000 s. To our knowledge, this is the first demonstration of broadband photothermal detection using frequency combs.

## Results

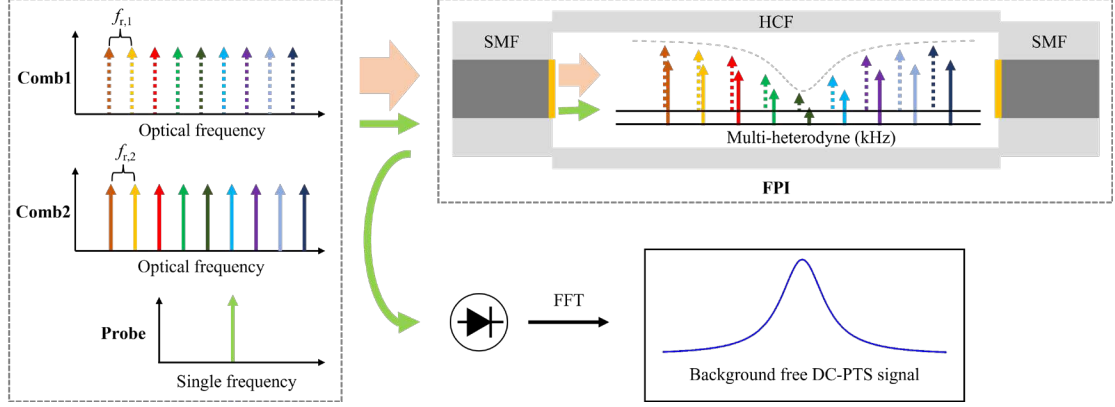


Fig. 1. Principle of dual-comb photothermal spectroscopy (DC-PTS). FPI: Fabry-Pérot interferometer; SMF: single mode fiber; HCF: hollow core fiber;  $f_{r,1}$ ,  $f_{r,2}$ : repetition frequencies of the two frequency combs; FFT: Fast Fourier Transform. Two frequency combs heterodyne against each other to provide a set of amplitude modulations at the down-converted evenly-spaced frequencies. The combs and a probe laser are coupled into a FPI formed by a HCF sandwiched by two solid-core SMFs. The refractive index of the target gas filled in the HCF is modulated by the pump comb source, leading to the phase modulation of the probe laser. The output of the probe laser from the FPI is used to retrieve the multi-heterodyne photothermal signal by Fourier transform.

**Theory.** Figure 1 presents the concept of the proposed DC-PTS. We use dual electro-optic frequency combs as the pump source for the proof-of-concept demonstration. The two OFCs with a set of discrete evenly-spaced and phase-coherent optical frequency components,  $f_{n,1}$  and  $f_{n,2}$ , can be expressed by

$$f_{n,1} = n \cdot f_{r,1} + f_0 + f_{shift,1} \quad (1)$$

$$f_{n,2} = n \cdot f_{r,2} + f_0 + f_{shift,2} \quad (2)$$

where  $n$  ( $0, \pm 1, \pm 2$ , etc.) is the comb line index;  $f_{r,j}$  and  $f_{shift,j}$  ( $j = 1$  and  $2$ ) are the repetition rate and optical frequency shift, respectively;  $f_0$  is the optical carrier frequency which is identical for the two combs when they are generated from the same source.

In DCS, one frequency comb heterodynes against the other to down-convert the optical frequencies into the radio frequency (RF) spectrum, which can be detected by a high-bandwidth photodetector. The difference of the two repetition rates and the difference of the optical frequency shifts determine the RF comb spacing and the center frequency of the RF spectrum, respectively. In this study, we tune the down-converted RF combs to a scope of tens of kHz so that the photothermal effect of gas-phase analyte can be efficiently excited after absorbing the comb light. The multi-heterodyne signal composes of distinguishable beatnotes between pairs of comb teeth at the radio frequency  $\nu_n$

$$\nu_n = |f_{n,1} - f_{n,2}| = n \cdot \Delta f_r + \Delta f_{shift} \quad (3)$$

where  $\Delta f_r = f_{r,1} - f_{r,2}$  and  $\Delta f_{shift} = f_{shift,1} - f_{shift,2}$ . Hence, the  $n^{\text{th}}$  comb line is modulated at the frequency  $\nu_n$ , acting as the  $n^{\text{th}}$  amplitude modulated pump laser. If this comb line is absorbed by the gas medium, the gas density (or refractive index) is modulated at the respective radio frequency  $\nu_n$ . As a result, a probe laser that is made collinear with the pump combs experiences a phase modulation at  $\nu_n$ . When the comb lines that can be absorbed by the gas molecules pass through the gas medium, the complex phase modulation signal can be detected by an optical interferometer and Fourier transformed to a photothermal spectrum.

As introduced previously, it is quite attractive to perform PTS in a HCF due to its highly efficient light-gas interaction and the significantly increased light intensity within the hollow core of a  $\mu\text{m}$ -sized MFD. For gas absorption by the  $n^{\text{th}}$  pair of comb teeth, the induced phase change for the probe laser along the HCF can be expressed by [27]

$$\Delta\phi_n = k^* AL \overline{\chi P}_{pump,n} \quad (4)$$

where  $k^*$  is a coefficient inversely proportional to the cross-section area of the mode field of the HCF,  $A$  is the peak absorption coefficient,  $L$  is the length of HCF,  $\overline{\chi}$  is the normalized line-shape function of the absorption feature,  $\overline{P}_{pump,n}$  is the square root of a product of the optical power levels for the  $n^{\text{th}}$  pair of comb teeth propagating through the HCF.

**Experimental setup.** Figure 2 depicts the experimental setup of PT-DCS based on an all-fiber electro-optic dual-comb source. The two combs generated from the same continuous wave (CW) external-cavity diode laser (ECDL) are designed with repetition rates of 500 MHz and 500.0001 MHz, and optical frequency shifts of 25 MHz and 25.03 MHz, respectively (See Methods). The dual-comb light is divided into two branches, one of which is used as the photothermal pump. A portion of the comb light is monitored by a photodetector to provide a synchronous reference for normalizing the possible non-uniform comb intensity distribution over a broad bandwidth (See Methods). The FPI used in this work consists of a 1572 nm probe laser, and a hollow-core anti-resonant fiber (HC-ARF) sandwiched by two SMFs. The HC-ARF also acts as a gas cell with a length of 7 cm, an air core diameter of 28  $\mu\text{m}$  and a diameter of holey region of 56  $\mu\text{m}$ , providing a gas sampling volume of only 0.17  $\mu\text{L}$ . The densely packed beatnotes centered at 30 kHz have a frequency span from 15 kHz to 45 kHz and a line spacing of 100 Hz, over which the FPI has a relatively high and flat-top response (See Supplementary).

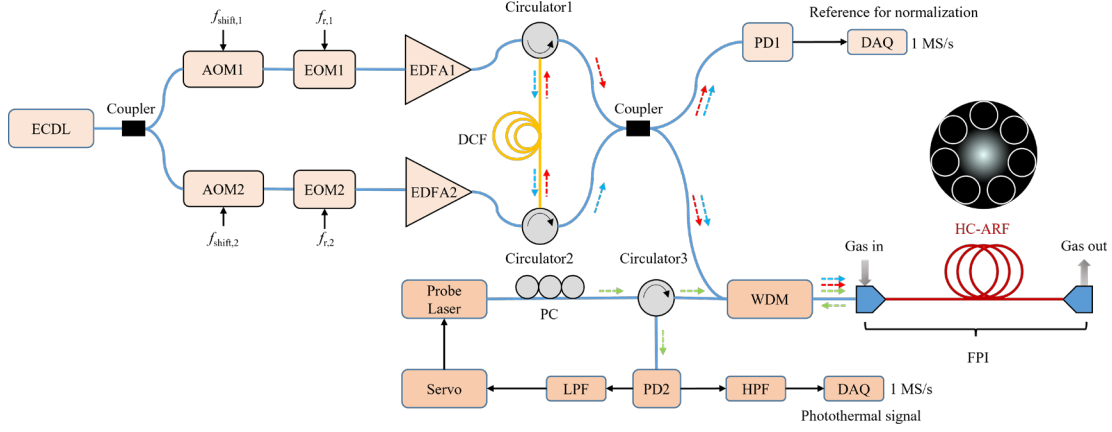


Fig. 2. Schematic of the DC-PTS setup. ECDC, external cavity diode laser; AOM, acousto-optic modulator; EOM, electro-optic modulator; EDFA, erbium doped optical fiber amplifier; DCF, dispersion compensation fiber; PD, photodetector; WDM, wavelength division multiplexer; PC, polarization controller; FPI, Fabry-Pérot interferometer; LPF, low-pass filter; HPF, high-pass filter; DAQ, data acquisition with 16-bit vertical resolution. The inset is a schematic illustration of the hollow-core anti-resonant fiber (HC-ARF) cross-section. The pump combs and the probe laser are delivered into the FPI via a WDM. The FPI output of the probe laser carrying the phase modulation information is picked up by the WDM and a circulator (Circulator3). The low-frequency component of the photodetector signal (PD2) is used to lock the probe wavelength to the quadrature point of the interference fringe via a laser servo to obtain the largest frequency-to-amplitude conversion factor (See Supplementary). The PC is used to optimize the contrast of interference fringes. The high-pass filtered time-domain photothermal interferograms are digitized at a sampling rate of 1 MS/s and Fourier transformed to retrieve the spectrum.

We choose acetylene ( $C_2H_2$ ) as an example to demonstrate the DC-PTS concept. Firstly, a gas mixture of 2%  $C_2H_2/N_2$  is introduced to the HC-ARF and the optical carrier frequency of the comb source is tuned to 195.444 THz. All the measurements are conducted at 1 bar and 296 K. Figure 3 (a) shows the representative time-domain interferograms. The bursts reproduce with a periodicity of 10 ms, corresponding to the repetition frequency difference of the dual-comb source. Figure 3 (b) shows the Fourier-transformed photothermal signal of  $C_2H_2$ , showing a comb-line-resolved spectrum over 15–45 kHz RF domain. One can easily distinguish two strong absorption lines P(15) and P(14) centered at  $\sim 25$  kHz (195.42 THz in optical domain) and  $\sim 41$  kHz (195.50 THz in optical domain), respectively; as well as two relatively weak lines at  $\sim 21$  kHz (195.40 THz) and  $\sim 35.4$  kHz (195.47 THz), respectively. It is of interest to observe one single comb line at 30 kHz, which is located at the far wing of the P(15) line. This comb line derives from the beatnote of the residual carrier CW lasers, leading to a much higher intensity than any other bilateral beatnotes. Such an influence can be mitigated by normalizing the direct photothermal measurement with a reference multi-heterodyne dual-comb signal using a photodetector, or by employing a pair of electro-optic modulators (EOMs) with a higher extinction ratio. We choose the former method in this study due to its simpler implementation. The inset graph of Fig. 3 (b) presents the multi-heterodyne dual-comb spectrum that is simultaneously recorded by the photodetector (PD1 in Fig. 2). Dividing the direct DC-PTS signal by the multi-heterodyne dual-comb spectrum, we can also mitigate the influence of the non-uniform intensity distribution of the comb source over a

broadband. In order to obtain the absorption features based on the HITRAN database, Fig. 3 (c) depicts the normalized  $C_2H_2$  spectrum for a measurement time of 10 s, which is in an excellent agreement (R-square value of 0.998) with the absorption spectral fitting using the HITRAN database [31].

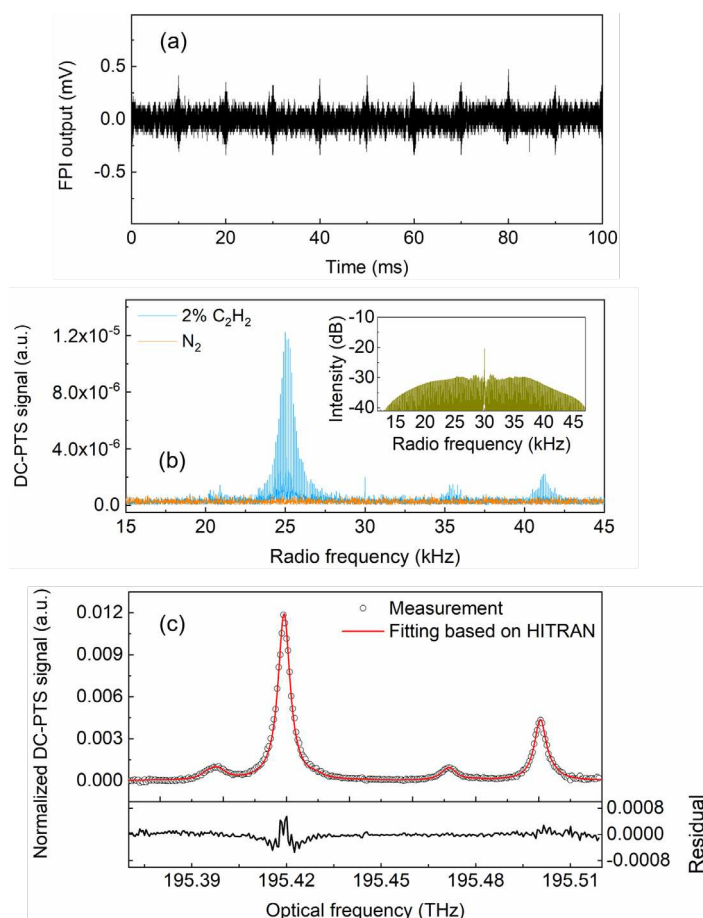


Fig. 3. Representative DC-PTS of  $C_2H_2$  measured at the central frequency of 195.444 THz. (a) Time-domain photothermal interferograms recorded by the FPI. (b) Fourier-transformed photothermal multi-heterodyne signal of 2%  $C_2H_2$  and pure  $N_2$  for a measurement time of 100 ms. The inset shows the corresponding dual-comb reference spectrum recorded by the photodetector PD1. (c) Normalized dual-comb photothermal spectrum of  $C_2H_2$  for a measurement time of 10 s. The residual between the measurement and spectral fitting is plotted at the bottom panel.

**Linear response and broadband detection.** We then evaluate the sensor response by measuring  $C_2H_2/N_2$  mixtures with different concentrations. A stronger absorption line P(11) is targeted by tuning the central frequency to 195.764 THz. A comb power of 15 mW is delivered to the HC-ARF in this test. Different gas mixtures are generated by diluting the certified 2%  $C_2H_2/N_2$  with  $N_2$  using a gas dilution system. The variation of the amplitude of the DC-PTS signal with  $C_2H_2$  concentration is plotted in Fig. 4, showing an excellent linear relationship (R-square value of 0.999).

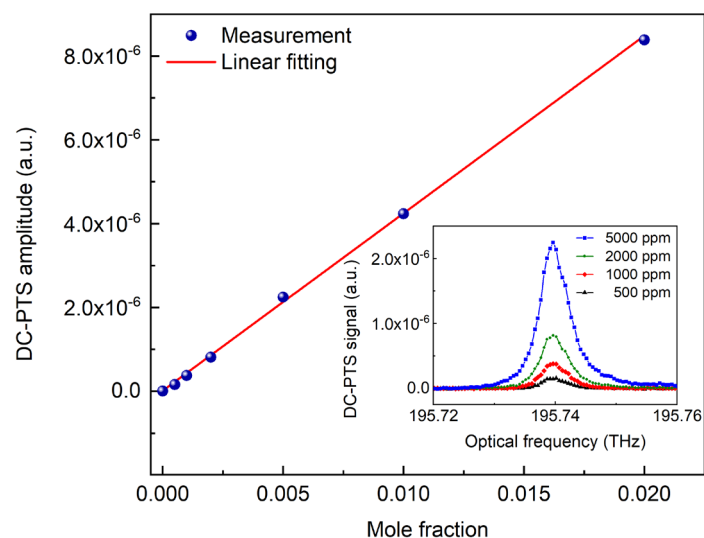


Fig. 4. Variation of the DC-PTS amplitude with gas concentration. The DC-PTS system shows an excellent linear response with an R-square value of 0.999. Inset: representative DC-PTS spectra of  $C_2H_2$  with different concentrations.

By tuning the ECDL frequency in a step-wise manner, the current electro-optical dual-comb spans more than 1 THz. For the gas sample of 2%  $C_2H_2/N_2$ , each DC-PTS measurement with normalization is conducted for a measurement time of 100 s, and then the spectral stitching is applied to obtain the entire spectra shown in Fig. 5. The rovibrational lines of the  $(\nu_1+\nu_3)$  band of  $C_2H_2$  are well-resolved in this spectral range, showing a good agreement with the simulated spectrum using the HITRAN database.

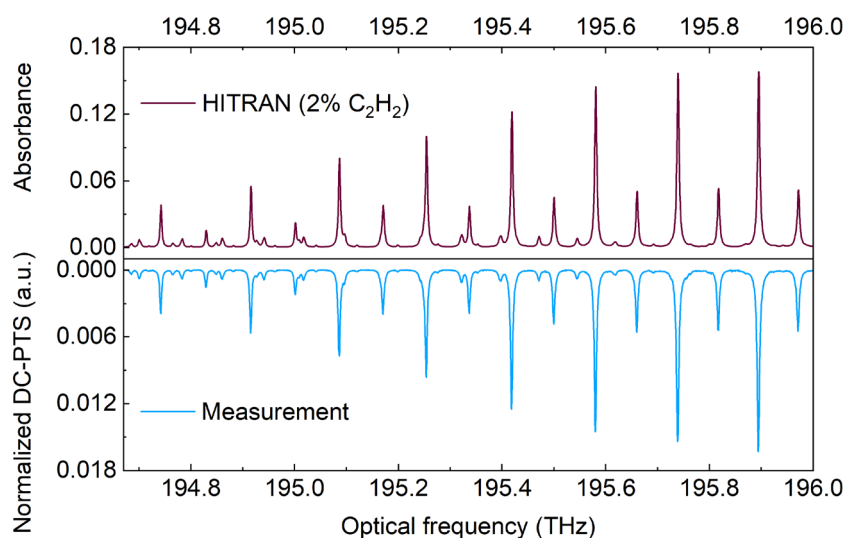


Fig. 5. Comparison of the broadband DC-PTS measurement with the spectral simulation based on the HITRAN database. The gas mixture of 2%  $C_2H_2$  is used in this test. The multi-heterodyne photothermal signal is normalized to account for the non-uniform comb intensity distribution and FPI response over a broadband.

## Discussion

The reported results reveal that the DC-PTS system provides a new way of dual-comb

spectroscopic measurements. It is of interest to discuss the possible methods of obtaining a higher signal-to-noise ratio (SNR) so that the DC-PTS can become more feasible for trace gas detection.

Firstly, the dependence of the DC-PTS signal on the pump power is studied. Here the pump power is measured at the coupler output of the two combined combs. By adjusting the pump power between 1 mW and 15 mW, Fig. 6 plots the corresponding amplitude of the DC-PTS signal measured for 10 s. The amplitude increases linearly with power. The commercial EDFA with a higher gain has achieved an output power of 1.5 W for gas sensing [32]. Considering the comb power of 15 mW used in this work, we expect to increase the sensitivity by two orders of magnitude.

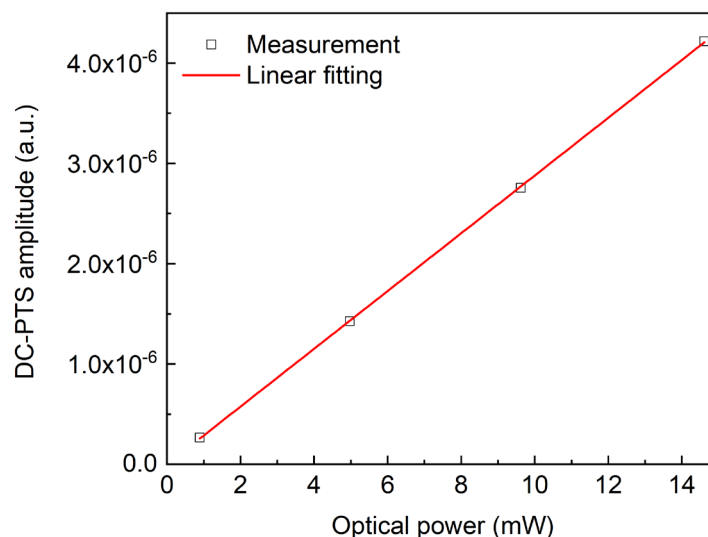


Fig. 6. Variation of the amplitude of DC-PTS signal with the comb power. The P(11) line of  $C_2H_2$  is analyzed for a measurement time of 10 s.

We further investigate the SNR by varying the measurement time. The definition of SNR can be found in Methods. Figure 7 illustrates that the SNR increases linearly with the square root of time from 10 ms up to 100 s, and further increases until the maximum recording duration of 1000 s with a slight deviation from the ideal trend line. Such a slight deviation at a longer measurement time may derive from the phase noise of combs caused by low-frequency temperature variation and mechanical vibration. For a mixture of 2%  $C_2H_2/N_2$ , the current DC-PTS system achieves a SNR of  $\sim 1100$  at the measurement time of 100 s, and  $\sim 2300$  at 1000 s. Hence, a minimum detection limit (MDL,  $1\sigma$ ) of 8.7 ppm is determined for the comb power of 15 mW, the fiber length of 7 cm, and the measurement time of 1000 s. It should be noted that such a long-term averaging method may be not suitable for applications that require a fast time response.

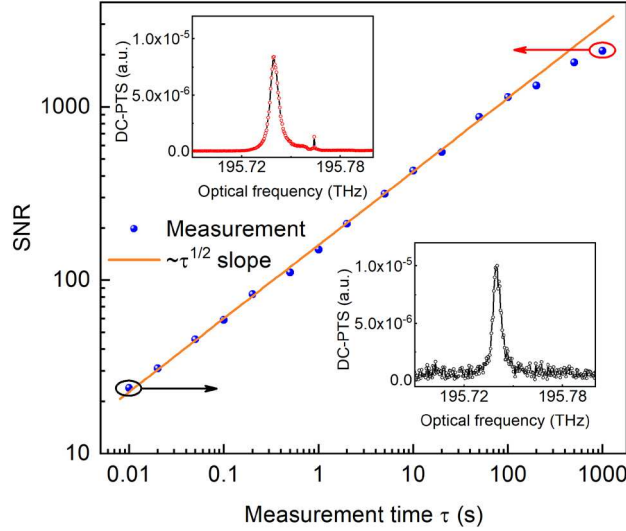


Fig. 7. Variation of the SNR of 2%  $C_2H_2$  with the measurement time. The measurement SNR is defined as the ratio of the peak magnitude of the PT response to the standard deviation of the non-absorption baseline. Insets: typical DC-PTS spectra measured at 10 ms and 1000 s, respectively.

Finally, we mention several other methods that can further enhance the system performance. For the electro-optic combs used in this work, it is feasible to change the comb spacing by tuning the repetition rate of the electrical pulse used for driving EOMs. We expect a repetition frequency of up to 5 GHz, which is mainly limited by the bandwidth of the pulse generator. A higher SNR can be obtained by increasing the repetition frequency as the power of each individual comb tooth rises with the increased line spacing, given a constant average power. However, we must consider a tradeoff between the measurement SNR and spectral resolution in actual spectroscopic measurements. Additionally, we use an HCF with a length of only 7 cm in this work. As the phase modulation can be accumulated with the fiber length shown in Eqn. (4), it is possible to increase the SNR by simply using a longer HCF. It has been recently reported that silica HC-ARFs have achieved a record low transmission loss of 0.28 dB/km in the C and L bands [33]. Hence, we expect to enhance the sensitivity by another two orders of magnitude if such a 10-m long HC-ARF is used for the FPI, considering its negligible loss of pump comb power.

In summary, we report the concept and proof-of-principle demonstration of DC-PTS using electro-optic dual-combs combined with an in-line FPI. Because of the inherently high mutual coherence of this dual-comb source and the exquisite frequency agility, the combined dual-combs generate the multi-heterodyne modulation of the RI of the gas sample filled in the HC-ARF. A moderate optical span of hundreds of GHz is mapped to the response frequency of the FPI. The photothermal spectra of  $C_2H_2$  pumped by the dual-comb source can be obtained by the Fourier transform of the interferograms generated from the FPI within a short measurement time, i.e., as short as 10 ms in this work. The spectra of  $C_2H_2$  over 1 THz are stitched by simply tuning the optical frequency of the ECDL. We achieve a MDL of 8.7 ppm for the comb power of 15 mW and fiber length of 7 cm. Several strategies of further improving the SNR are discussed. Hence, our study opens a new opportunity to realize broadband, high-resolution and ultrasensitive chemical analysis. Although demonstrated for electro-optic combs, we believe it is quite promising to apply our technique for mid-infrared combs generated from micro-resonators [34], quantum cascade

lasers [35] and interband cascade lasers [36] with extra merits of stronger gas absorption and reduced size for intergration.

## Methods

### Electro-optic dual-comb source

For the generation of electro-optic dual-combs, a CW-ECDL is divided into two branches via a 50:50 fiber coupler and then each branch is connected in parallel to an acousto-optic modulator (AOM), which shifts the frequency of the CW laser by 25 MHz and 25.03 MHz, respectively. These two frequency-shifted optical beams are intensity modulated by two EOMs, driven by 50-ps pulses at slightly different repetition frequencies of 500 MHz and 500.0001 MHz, respectively. The generated pulse trains are amplified by EDFAs and subsequently counter launched into a single 1-km nonlinear optical fiber with high normal dispersion (dispersion of  $-130 \text{ ps}\cdot\text{nm}^{-1}\cdot\text{km}^{-1}$ , and low dispersion slope of  $-0.15 \text{ ps}\cdot\text{nm}^{-2}\cdot\text{km}^{-1}$ ) for spectral broadening. The broadened combs are separated by a pair of circulators (Circulator1 and Circulator2 shown in Fig. 2) at each end of the nonlinear fiber. The dual combs are mixed and split into two beams by a coupler for photothermal pumping and normalization purposes, respectively.

### In-line Fabry-Pérot interferometer

By mechanically splicing a HCF to an input SMF pigtail and an output SMF pigtail, a FPI can be formed by natural reflections at the two joints between the HCF and SMFs [37]. The relative position between facets of the two kinds of fibers are finely adjusted to achieve a maximum contrast of interference for the probe laser. For gas inlet and outlet, both joints have a gap of 1–2  $\mu\text{m}$  and are sealed within a T-shaped glass tube. The HCF also acts as a gas cell in the interferometer. We use a HC-ARF with a length of 7 cm instead of the commercial hollow-core photonic band-gap fiber (HC-PBF). Such a new fiber exhibits a relatively larger air core (28  $\mu\text{m}$ ) to facilitate the gas loading and the total gas consumption is only 0.17  $\mu\text{L}$ . The mode purity of the HC-ARF is much better and mode interference noise is essentially avoided by careful alignment of the input SMF and the HC-ARF.

### Photothermal spectral analysis

The direct DC-PTS signal is shown in Fig. 3(b). However, the photothermal effect is proportional to the pump comb power shown in Fig. 6. Thus, the original DC-PTS signal is convolved by the effects of the non-flat FPI response (see Supplementary Fig. S2) and non-uniform power distribution of comb lines. Based on the tooth-to-tooth mapping relationship, the direct DC-PTS signal is normalized to the intensity of the dual-comb spectrum and the response of the FPI.

### SNR definition

The SNR is defined as the peak value of the retrieved P(11) line divided by the standard deviation of the signal in the range of 195.77–195.80 THz, where the absorption of  $\text{C}_2\text{H}_2$  is minimal. The radio-frequency scale is converted to an optical scale based on the frequency compression factor of  $f_r/\Delta f_r = 5 \times 10^6$ , as well as the knowledge of the optical carrier frequency.

### Data availability

The data that support the findings within this paper are available from the corresponding authors upon reasonable request.

## References

1. Udem, T., Holzwarth, R. & Hänsch, T. Optical frequency metrology. *Nature* **416**, 233-237 (2002).
2. Cundiff, S. T. & Ye, J. Colloquium: Femtosecond optical frequency combs. *Rev. Mod. Phys.* **75**, 325-342 (2003).
3. Baltuška, A., Udem, T., Uiberacker, M. et al. Attosecond control of electronic processes by intense light fields. *Nature* **421**, 611-615 (2003).
4. Torres-Company, V. & Weiner, A. M. Optical frequency comb technology for ultra-broadband radio-frequency photonics. *Laser Photonics Rev.* **8**, 368-393 (2014).
5. Grinin, A., et al. Two-photon frequency comb spectroscopy of atomic hydrogen. *Science* **370**, 1061-1066 (2020).
6. Maddaloni, P., Bellini, M. & de Natale, P. Laser-Based Measurements for Time and Frequency Domain Applications: A Handbook (CRC Press, Boca Raton, 2013).
7. Picqué, N. & Hänsch, T. W. Frequency comb spectroscopy. *Nat. Photon.* **13**, 146-157 (2019).
8. Coddington, I., Newbury, N. & Swann, W. Dual-comb spectroscopy. *Optica* **3**, 414-426 (2016).
9. Foltynowicz, A., Ban, T., Maslowski, P., Adler, F. & Ye, J. Quantum-noise-limited optical frequency comb spectroscopy. *Phys. Rev. Lett.* **107**, 233002 (2011).
10. Thorpe, M. J., Moll, K. D., Jones, J. J., Safdi, B. & Ye, J. Broadband cavity ringdown spectroscopy for sensitive and rapid molecular detection. *Science* **311**, 1595-1599 (2006).
11. Thorpe, M. J. & Ye, J. Cavity-enhanced direct frequency comb spectroscopy. *Appl. Phys. B* **91**, 397-414 (2008).
12. Bernhardt, B. et al. Cavity-enhanced dual-comb spectroscopy. *Nat. Photon.* **4**, 55-57 (2010).
13. Chen, Z., Yan, M., Hänsch, T. & Picqué, N. A phase-stable dual-comb interferometer. *Nat. Commun.* **9**, 3035 (2018).
14. Suh, M.-G., Yang, Q.-F., Yang, K. Y., Yi, X. & Vahala, K. J. Microresonator soliton dual-comb spectroscopy. *Science* **354**, 600-603 (2016).
15. Ideguchi, T. et al. Adaptive real-time dual-comb spectroscopy. *Nat. Commun.* **5**, 3375 (2014).
16. Villares, G., Hugi, A., Blaser, S. & Faist, J. Dual-comb spectroscopy based on quantum-cascade-laser frequency combs. *Nat. Commun.* **5**, 5192 (2014).
17. Zhao, X. et al. Picometer-resolution dual-comb spectroscopy with a free-running fiber laser. *Opt. Express* **24**, 21833-21845 (2016).
18. Ycas, G. et al. High-coherence mid-infrared dual-comb spectroscopy spanning 2.6 to 5.2  $\mu\text{m}$ . *Nat. Photonics* **12**, 202-208 (2018).
19. Muraviev, A. V., Smolski, V. O., Loparo, Z. E. & Vodopyanov, K. L. Massively parallel sensing of trace molecules and their isotopologues with broadband subharmonic mid-infrared frequency combs. *Nat. Photonics* **12**, 209-214 (2018).
20. Yan, M. et al. Mid-infrared dual-comb spectroscopy with electro-optic modulators. *Light Sci. Appl.* **6**, e17076 (2017).
21. Zhang, W., Chen, X., Wu, X., Li, Y. & Wei, H. Adaptive cavity-enhanced dual-comb spectroscopy. *Photonics Res.* **7**, 883-889 (2019).
22. Hoghooghi, N., Wright, R.J., Makowiecki, A.S., Swann, W.C., Waxman, E.M., Coddington, I. & Rieker, G.B., Broadband coherent cavity-enhanced dual-comb spectroscopy. *Optica* **6**, 28-33 (2019).
23. Sadiq, I., Mikkonen, T., Vainio, M., Toivonen, J., & Foltynowicz, A. Optical frequency comb photoacoustic spectroscopy. *Phys. Chem. Chem. Phys.* **20**, 27849-27855 (2018).
24. Karhu, J. et al. Broadband photoacoustic spectroscopy of  $^{14}\text{CH}_4$  with a high-power mid-infrared optical

- frequency comb. *Opt. Lett.* **44**, 1142-1145 (2019).
25. Wildi, T., Voumard, T., Brasch, V., Yilmaz, G., & Herr, T. Photo-acoustic dual-frequency comb spectroscopy. *Nat. Commun.* **11**, 4164 (2020).
  26. Friedlein, J. T. et al. Dual-comb photoacoustic spectroscopy. *Nat. Commun.* **11**, 3152 (2020).
  27. Jin, W., Cao, Y., Yang, F. & Ho, H. L. Ultra-sensitive all-fibre photothermal spectroscopy with large dynamic range. *Nat. Commun.* **6**, 7767 (2015).
  28. Heylman, K. D. et al. Optical microresonators as single-particle absorption spectrometers. *Nat. Photon.* **10**, 788-795 (2016)
  29. Zhao, P., Zhao, Y., Bao, H., Ho, H. L., Jin, W., Fan, S., Gao, S., Wang, Y. & Wang, P. Mode-phase-difference photothermal spectroscopy for gas detection with an anti-resonant hollow-core optical fiber. *Nat. Commun.* **11**, 847 (2020).
  30. Boyer, D., Tamarat, P., Maali, A., Lounis, B. & Orrit, M. Photothermal imaging of nanometer-sized metal particles among scatterers. *Science* **297**, 1160-1163 (2002).
  31. Gordon, I. E., Rothman, L. S., Hill, C., Kochanov, R. V., Tan, Y., Bernath, P. F., Birk, M., Boudon, V., Campargue, A., Chance, K. V., Drouin, B. J., Flaud, J. M., Gamache, R. R., Hodges, J. T., Jacquemart, D., Perevalov, V. I., Perrin, A., Shine, K. P., Smith, M. -A. H., Tennyson, J., Toon, G. C., Tran, H., Tyuterev, V. G., Barbe, A., Császár, A. G., Devi, V. M., Furtenbacher, T., Harrison, J. J., Hartmann, J. M., Jolly, A., Johnson, T. J., Karman, T., Kleiner, I., Kyuberis, A. A., Loos, J., Lyulin, O. M., Massie, S. T., Mikhailenko, S. N., Moazzen-Ahmadi, N., Müller, H. S. P., Naumenko, O. V., Nikitin, A. V., Polyansky, O. L., Rey, M., Rotger, M., Sharpe, S. W., Sung, K., Starikova, E., Tashkun, S. A., Auwera, J. V., Wagner, G., Wilzewski, J., Weislo, P., Yu, S. & Zak, E. J. The HITRAN2016 molecular spectroscopic database. *J. Quant. Spectrosc. Radiat. Transfer* **203**, 3-69 (2017).
  32. Wu, H., Sampaolo, A., Dong, L., Patimisco, P., Liu, X., Zheng, H., Yin, X., Ma, W., Zhang, L. & Yin W. Quartz enhanced photoacoustic H<sub>2</sub>S gas sensor based on a fiber-amplifier source and a custom tuning fork with large prong spacing. *Appl. Phys. Lett.* **107**, 111104 (2015).
  33. Jason, G. T. et al. Hollow core NANF with 0.28 dB/km attenuation in the C and L bands. *Optical Fiber Communication Conference* p Th4B.4, Optical Society of America, (2020).
  34. Shen, B. et al. Integrated turnkey soliton microcombs. *Nature* **582**, 365-369 (2020).
  35. Hugé, A. et al. Mid-infrared frequency comb based on a quantum cascade laser. *Nature* **492**, 229-233 (2012).
  36. Bagheri, M. et al. Passively mode-locked interband cascade optical frequency combs. *Sci. Rep.* **8**, 1-7 (2018).
  37. Yang, F., Tan, Y., Jin, W., Lin, Y., Qi, Y., & Ho, H. L. Hollow-core fiber Fabry–Perot photothermal gas sensor. *Opt. Lett.* **41**, 3025-3028 (2016).

## Acknowledgements

This research was supported by the National Natural Science Foundation of China (NSFC) (62005267, 51776179), Strategic Priority Research Program of Chinese Academy of Sciences (XDA17040513, XDA22020502), General Research Fund (14209220) from the University Grants Committee, Innovation and Technology Fund (MHP/049/19, GHP/123/19GD) from the Innovation and Technology Commission, Scientific Instrument Developing Project of the Chinese Academy of Sciences (YJKYYQ20190037), the Second Comprehensive Scientific Investigation of the Qinghai-Tibet Plateau (2019QZKK020802).

## Author contributions

Q.W., Z.W. and W.R. conceived the idea, designed the experiments, discussed the results and prepared the manuscript. Q.W. built the systems and conducted the experiments. Z.W. assisted in building the systems and

conducting the experiments. H.Z. completed the spectral analysis. S.J. and W.J. fabricated the fiber-based interferometer. Y.W. provided the hollow core anti-resonant fiber. Q.W. and W.R. supervised and coordinated the project.

### **Competing interests**

The authors declare no competing interests.

### **Additional information**

Supplementary information is available for this paper.

Correspondence and requests for materials should be addressed to Q.W., Z.W. or W.R.

## Supplementary Files

This is a list of supplementary files associated with this preprint. Click to download.

- [Supplementary.docx](#)